Advances in Astronomy and Space Physics, **9**, 8-13 (2019) doi: 10.17721/2227-1481.9.8-13

X-ray scaling relations of elliptical galaxies

*Iu. V. Babyk**

Main Astronomical Observatory of the National Academy of Sciences of Ukraine, 27 Zabolotnoho str., 03143, Kyiv, Ukraine
Department of Physics and Astronomy, University of Waterloo, 200 University Avenue West, Waterloo, ON N2L 5G1, Canada
Waterloo Institute for Astrophysics, University of Waterloo, 200 University Avenue West, Waterloo, ON N2L 5G1, Canada

We present the X-ray scaling relations of a sample of elliptical galaxies using X-ray Chandra observations. We use a single β-model to reconstruct the density gas profile and the hydrostatic equation to measure the total mass. We build X-ray scaling relations between temperature, luminosity and total mass at $5R_e$. Our sample includes gas-poor objects that help us to extend already published $L_X - T$, $M - T$ and $L_X - M$ scaling relations to lower magnitudes. The derived slopes for all three relations are much steeper than those for galaxy clusters and groups, and are extreme compared to self-similar models considering gravity only. This increase of steepness from clusters to galaxies indicates that non-thermal processes (e.g. AGN feedback) have a stronger influence on the small-scale systems. Our results indicate that the hot interstellar medium of gas-poor early-type galaxies is not in the wind/outflow state as suggested by recent hydrodynamical simulations. We also discuss the possible biases of our calculations and compare our results to recent papers.

Key words: galaxies: elliptical and lenticular, cD; galaxies: evolution; galaxies: formation

INTRODUCTION

Besides the well-established Fundamental Plane, Faber-Jackson, Kormendy, and colour-magnitude scaling relations, the X-ray galaxy scaling relations can be intensively used as a probe of galaxy structure and evolution. Recent X-ray scaling relation studies have been performed mostly for the relations between optical and X-ray luminosity which links the stellar mass with their X-ray luminosity. They have been widely used to explore the origin and evolution of the interstellar medium (ISM) of early-type galaxies (ETGs). ETGs (elliptical and lenticular, E & S0) host atmospheres of hot diffuse gas [28]. They are mostly old systems and consist of old, red-giant stars. However, they also demonstrate little star formation activity [29]. Moreover, recent observational results showed the detection of cold molecular gas and dust in ETGs [4, 14].

The ΛCDM model predicts that gravitational structures, such as clusters, groups, and individual galaxies have been formed similarly from small density fluctuations and that their properties, such as temperature, luminosity and mass should scale similarly as well. According to the self-similar theory [15], the luminosity should scale with temperature as $L_X \propto T^2$, the mass with temperature as $M \propto T^{3/2}$, while luminosity scales with mass as $L_X \propto M^{4/3}$. However, it is well-established that the observational properties of clusters show significant deviations compared to theory. The previous studies of galaxy clusters provide $L_X \propto T^{2.7-3}$ and $M \propto T^{1.7-2}$ [15]. Moreover, the less massive and colder systems such as groups and galaxies demonstrate stronger deviations, e.g., $L_X \propto T^{3-4}$ and $L_X \propto T^{4.5-5}$, whilst $M \propto T^{2-2.2}$ and $M \propto T^{2-2.4}$ for groups and galaxies respectively [3, 16, 17, 29]. The cluster scaling relations have been intensively studied over the last decade, while small mass-scale systems was disregarded due to the low quality of the past X-ray instruments. Thus, our main motivation of this paper is the study of a homogeneous sample of individual, elliptical galaxies to explore their X-ray scaling relations and to compare them with theoretical predictions.

The observed deviations in X-ray scaling relations are the evidence of non-gravitational processes occurring in the cores of galaxy clusters (namely at the core of brightest cluster galaxy (BCGs)), groups (brightest group galaxy (BGGs)) and individual galaxies. There are many known non-gravitational processes, e.g., AGN feedback, shock heating, stripping, etc., but it is not clear which one is fundamental and how exactly these processes operate inside the intracluster, intragroup, and interstellar media. The most plausible mechanism for causing the

*babikyura@gmail.com

deviations in X-ray scaling relations is AGN feedback [13, 20, 27]. According to this mechanism, the accretion of matter onto a supermassive black hole (SMBH) produces a jet of relativistic plasma which heats the surrounding environment and inflates X-ray cavities (the bubbles of matter with lower density compared to surrounding gas). These cavities rise buoyantly and are found using X-ray and radio observations of clusters, groups, and individual galaxies as well. The understanding of AGN feedback is important since it implicated in scaling relations and the formation of cosmic structures used in cosmological probes [3, 16–18, 22, 23].

Recent numerical simulations of scaling relations with AGN feedback models have provided additional evidence of the presence of non-gravitational processes within cluster-group-galaxy cores [5]. All these processes can provide additional heating at the cores of hot atmosphere structures. Thus, the origin of heating in the hot atmospheres of wide-mass-scale systems via the AGN feedback influence is a focus of this paper.

Recent and past X-ray scaling relations have been performed mostly for galaxy clusters only. The X-ray scaling relations for objects with lower mass, such as groups and galaxies, are less studied.

In our recent work [3] we performed the detailed study of the scaling relations for low-mass systems, including early- and late-type galaxies, cD, brightest cluster galaxies as well as faint and bright groups of galaxies. We obtained significant results, i.e., several scaling relations between temperature, gas mass, luminosity, total gravitational mass, etc. We got steeper slopes compared to the theoretical predictions almost for all scaling relations, indicating on the powerful influence of non-thermal heating processes (as e.g., AGN feedback) in our sample. However, our scaling relations showed significant scatter. This paper is an extension of the recent one. Here we check the cause for such a high scatter obtained in [3] for three main scaling relations, $L_X - T$, $M - T$, and $L_X - M$. We are trying to check whether the heterogeneity of the sample in our previous paper was a cause of such a high scatter or not. In addition, we are also checking the difference between the slopes for these three relations. For this purpose we select galaxies with the similar morphological type, namely only elliptical (see Table 1), perform similar data and spectral analysis as in [3], and plot three main scaling relations to compare the slopes and scatters between the previous and new relations.

The X-ray and optical data reduction, as well as the spectral modelling, are presented in details in our recent paper [3]. Here, we summarise it briefly.

L_X–T RELATION

The X-ray temperature for objects of our sample was derived from their spectra within $5R_e$. The temperature of elliptical galaxies varies from 0.2 keV to about 1.3 keV. Unabsorbed X-ray fluxes were used to obtain the X-ray luminosity as $L_X = 4\pi D_L^2 f_X$. Our sample spans four orders of magnitude of X-ray luminosity, 10^{38}–10^{42} erg/s.

Our X-ray temperature and luminosity measurements agree well with recent Chandra and XMM-Newton estimates presented in [12, 17, 29]. We found an insignificant systematic discrepancy for the temperature values. This discrepancy might be due to: (i) usage of the C-statistic in our `xspec` spectral analysis while quoted authors used χ^2 statistic; (ii) considering slightly different fixed parameters in our multi-component model; (iii) and/or using different energy bands during spectral modelling.

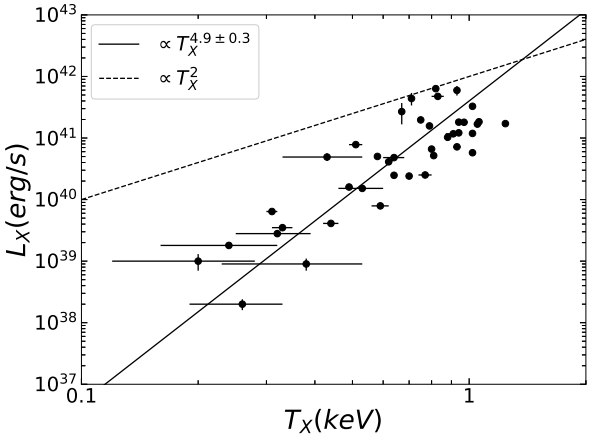

Fig. 1: The luminosity plotted against temperature. The solid line represents the best-fit model, while the dashed line corresponds to the theoretically predicted self-similar scaling.

Our defined $L_X - T$ relation is shown in Fig. 1. We applied the bivariate correlated error and intrinsic scatter (BCES) algorithm [1] to define the form of the $L_X - T$ scaling relation. This orthogonal algorithm performs a linear least-squares regression. This regression minimises the orthogonal distance to the best-fit relation. Uncertainties for the best-fit parameters were measured by 10000 Monte Carlo bootstrap re-samplings. The best-fitting $L_X - T$ relation for our sample is $L_X \propto T^{4.9\pm0.3}$. Our relation spans over a wide band of X-ray luminosity ($\sim 10^{38}$–10^{42} erg/s) and temperature ($\sim$ 0.1–1.2 keV). The hotter and more luminous objects in our sample, BCGs, occupy the top-right corner of the plot. The red dashed line shows the scaling predicted according to the self-similar theory. Our observed $L_X - T$ relation is significantly steeper than the self-similar prediction. This steepness indicates the significance of baryon physics on both small and large scales. The $L_X - T$ relation of galaxy clusters are shallower than in groups and elliptical galaxies. This means

that non-gravitational processes are more efficient in low-mass systems.

M–T AND L_X–M RELATIONS

The $M-T$ scaling relation is more fundamental than L_X-T since the mass of cosmic structures has been widely used to define cosmological parameters [9, 21, 31] and the mass function helps to clarify the cosmology of the Universe as well [10, 30].

We use a simple β-model [6] and the equation of hydrostatic equilibrium to describe the X-ray surface brightness profiles and to calculate the total mass of the elliptical galaxies. We extract the X-ray surface brightness profiles from the background-subtracted images. Each surface profile was centred on the peak X-ray emission and contained 100 annular regions of uniform width. The background subtraction was performed similarly as for optical surface brightness profiles. The background-subtracted surface profiles were then fitted with a single β-model as

$$S(r) = S_0 \left(1 + \left(\frac{r}{r_c}\right)^2\right)^{-3\beta+1/2} + C,$$

where $S(r)$ is the X-ray surface brightness as a function of projected radius. S_0, r_c, β, and C are free parameters in the model. The typical best-fit slope for elliptical galaxies varies as $\beta \approx 0.45$–0.50, which is smaller than the ~ 0.6–0.7 for galaxy clusters. The total gravitating mass was estimated assuming hydrostatic equilibrium of hot gas, its spherical symmetry and isothermality (T is constant)

$$M = -\frac{kTr}{G\mu m_p}\left(\frac{\mathrm{d}\ln\rho_g}{\mathrm{d}\ln r}\right),$$

where G is the gravitational constant, $\rho_{\rm g}$ is the gas density, and M is the total mass inside a sphere of radius r, $\mu = 0.62$ is the mean molecular weight of the hot gas and m_p is the mass of a proton. We estimating the hot gas density using the β-model fits of our X-ray surface brightness profiles. The gas density was found as

$$\rho_{\rm g}(r) = \rho_0 \left(1 + \left(\frac{r}{r_c}\right)^2\right)^{-3\beta/2},$$

where r_c is the core radius and $\rho_0 = 2.21\mu m_p n_0$ is the central gas density (see [8] for more details).

On the left panel of Fig. 2 we show the $M-T$ relation for the entire sample of elliptical galaxies. The best-fit result is $M \propto T^{2.2\pm0.2}$. The theoretically predicted self-similar model suggests that the total mass should scale with temperature as $M \propto T^{3/2}$. Thus, we observe that our $M-T$ relation is also steeper than those predicted by self-similarity. However, the observed steepness is less significant than those for the L_X-T scaling relation. This is because the major amount of the X-ray luminosity is generated in the cores of low-mass systems. Our results are in agreement with [19, 26] who conclude that the total mass-temperature relation is less sensitive to the non-gravitational processes.

The scaling relation between X-ray luminosity and the total mass is presented on the right panel of Fig. 2. For the entire sample we obtained $L_X \propto M^{2.2\pm0.3}$. We found that the Malmquist bias is present in the relations with luminosity, L_X-T and L_X-M [30]. This bias is only related to the low-redshift sample. We considered this bias using $\delta \ln L_X = 3/2\sigma_i^2$ equation, where σ_i is an intrinsic scatter in the log-normal value of luminosity for a given T. We applied this bias to both L_X-M and L_X-M scaling relations. As a result, we observe an insignificant modification of normalisation of our fits. However, this bias does not affect the power-law slopes.

DISCUSSION

The comparison of the obtained slopes and scatter with our recent work [3] are presented in Table 2. The general trend in the slopes for all three scaling relations are similar within uncertainties to those obtained in [3]. However, we found shallower slopes for $M-T$ and L_X-M relations. Moreover, the scatter in our sample is much lower (about a factor of 2) than in used for [3]. The latter indicates the importance of the sample homogeneity in the scaling relation studies.

Table 2: Comparison of the best-fit parameters with our previous results from [3]

	Slope		Scatter	
	This work	[3]	This work	[3]
L_X–T	4.9 ± 0.3	4.4 ± 0.2	0.41	0.99
M–T	2.2 ± 0.2	2.4 ± 0.2	0.28	0.52
L_X–M	2.2 ± 0.3	2.8 ± 0.3	0.52	0.99

According to the self-similar model, the physical properties of different sized objects should scale similarly [23]. The observed deviations indicate that non-gravitational processes such as supernova heating, thermal conduction, stellar mass losses, AGN feedback, etc. occur in the cores of these systems. The hot ISM can be also influenced by the effects of shocks, accretion, sloshing, stripping, and other processes. Although it is known how and where these processes occur, the contribution and impact of each of them are still under debate. They all may contribute at some level. Since the most energetic/powerful source of heat in the cores of elliptical galaxies is AGN, the AGN feedback mechanism is likely the dominant process [20].

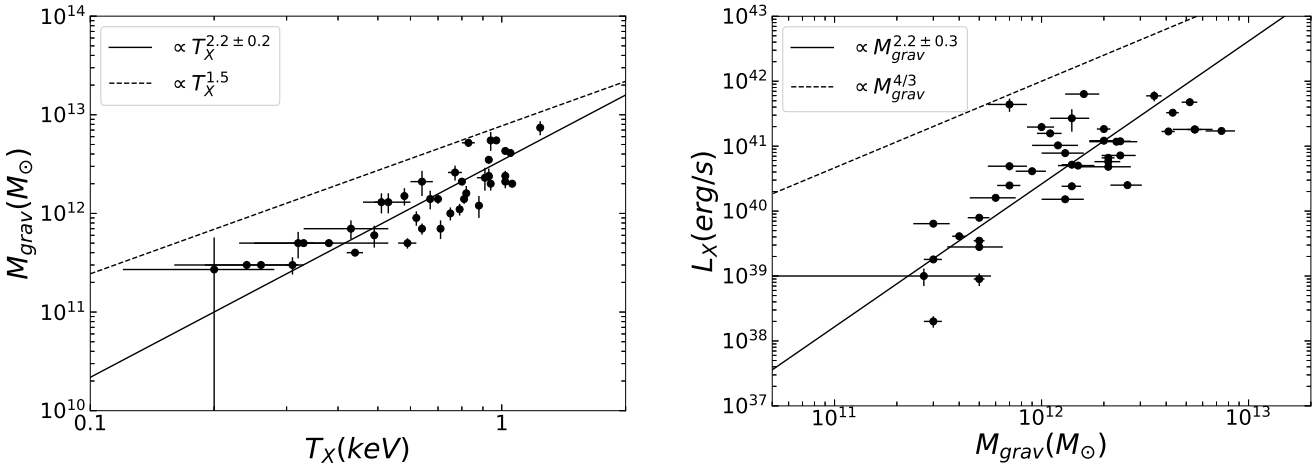

Fig. 2: The X-ray total mass plotted against temperature. The solid line corresponds to the best-fit, while the dashed line corresponds to the self-similar scaling (left panel). The X-ray luminosity plotted against total mass. The solid line corresponds to the best-fit, while the dashed line represents the self-similar theory (right panel).

During the last decade, theoretical and observational studies of galaxy clusters, groups, and early-type galaxies have revealed that feedback from AGN occurred in cores of these objects plays a significant role in the heating and cooling of the X-ray hot gas and provides deviations in the observed scaling relations discussed above. The galactic core contains larger amounts of X-ray diffuse gas, and it is able to transfer more energy into the interstellar environment via AGN feedback. Radio-mode AGN feedback is very efficient in providing the possible heating scenarios [20]. Mechanical AGN feedback produces X-ray cavities, shocks, and a metal increment along the radio jet that have been observed in the cores of clusters, groups, and individual galaxies.

Many theoretical models have been proposed to explain AGN feedback in clusters and galaxies [11]. By adding an AGN feedback models to observed scaling relations, the quoted authors were able to explain the observed deviations. In the paper [11] the authors applied their self-regulated AGN feedback model with stellar evolution to clusters, groups, and galaxies. As a result, they solved the cooling flow problem and were able to reproduce the various observational features, like buoyant cavities, subsonic turbulence, cold gas, etc. They showed that AGN feedback is less efficient and powerful for isolated galaxies than those in elliptical galaxies due to the influence of the intergalactic medium on the hot gas of elliptical galaxies.

It was performed the detailed hydrodynamic simulations of AGN feedback in elliptical galaxies in [25] as well. These authors focused on the observational properties of the interstellar medium, luminosity, and temperature in the soft and hard X-rays. As a result, they reproduced large variations of the X-ray luminosity that we observe in our analysis.

The origin of the hot gas in elliptical galaxies is still under debate. There are several proposed scenarios for the origin of hot gas in those objects, such as stellar loss and/or accretion of matter from the larger scales [12]. Following the ΛCDM model, hot gas in elliptical galaxies is shocked-heated. This gas cools slowly through its X-ray emission [2]. In paper [7] it was showed that hot gas density is less concentrated than the dark matter density using GIMIC simulations. This leads to the lower luminosity observed in halo of the late-type galaxies. 2D hydrodynamic simulations performed by [24] showed that hot gas with luminosity lower than $\sim 10^{40}$ erg/s is in a wind/outflow. They also predict higher temperatures at such low luminosity. However, we found no evidence of such high temperature in objects with low luminosity, confirming the recent result of [17].

CONCLUSIONS

We have found tight relations between luminosity, temperature, and mass of elliptical galaxies that indicate their self-regulated nature. Our best-fit results show steeper slopes than predicted from the self-similar theory. The main results and conclusions can be summarised as follows.

Our results for three X-ray scaling relations disagree with self-similar predictions, showing significantly steeper relations. These deviations indicate the presence of non-gravitational processes occurring in the hot atmosphere of elliptical galaxies.

We conclude that AGN feedback is likely the most important non-gravitational process that occurs in the cores of these sources and must be considered to resolve deviations between observed X-ray scaling relations and self-similar theory.

The tight $L_X - T$ correlation for low-luminosity objects (below 10^{39-40} erg/s) disagrees with hydro-

dynamical simulations which predict higher temperatures for galaxies with low-luminosity.

We also found that all scaling relations for our homogeneous sample of elliptical galaxies provide lower scatter during fitting in comparison with those obtained for all type of galaxies, including early-, late-types galaxies, BCGs, BGGs, cD, etc.

ACKNOWLEDGEMENT

The author is grateful to an anonymous referee for useful comments and suggestions that helped to improve the manuscript. This research was made using the data obtained from the Chandra Data Archive and the Chandra Source Catalogue, and software provided by the Chandra X-ray Center (CXC) in the application packages `CIAO`, `ChIPS`, and `Sherpa`. We thank all the staff members involved in the Chandra project.

REFERENCES

[1] Akritas M. G. & Bershady M. A. 1996, ApJ, 470, 706.
[2] Anderson M. E., Gaspari M., White S. D. M. et al. 2015, MNRAS, 449, 3806
[3] Babyk Iu. V., McNamara B. R., Nulsen P. E. J. et al. 2018, ApJ, 857, 32.
[4] Babyk Iu. V., McNamara B. R., Tamhane P. D. et al. 2018 [arXiv:1810.11465].
[5] Borgani S., Murante G., Springel V. et al. 2004, MNRAS, 348, 1078.
[6] Cavaliere A. & Fusco-Famiano R. 1978, A&A, 70, 677.
[7] Crain R. A., McCarthy I. G., Frenk C. S., Theuns T., Schaye J. 2010, MNRAS, 407, 1403.
[8] Ettori S. 2000, MNRAS, 318, 1041.
[9] Ettori S. 2013, MNRAS, 435, 1265.
[10] Finoguenov A., Reiprich T. H., and Böhringer H. 2001, A&A, 368, 749.
[11] Gaspari M., Brighenti F., Temi F. 2012, MNRAS, 424, 190.
[12] Goulding A. D., Greene J. E., Ma C.-P. et al. 2016, ApJ, 826, 167.
[13] Hogan M. T., McNamara B. R., Pulido F. A. et al. 2017, ApJ, 851, 66.
[14] Huang S. & Gu Q.-S. 2009, MNRAS, 398, 1651.
[15] Kaiser N. 1986, MNRAS, 222, 323.
[16] Kim D.-W. & Fabbiano G. 2013, ApJ, 776, 116.
[17] Kim D.-W. & Fabbiano G. 2015, ApJ, 812, 127.
[18] Kravtsov A. V., Vikhlinin A., and Nagai D. 2006, ApJ, 650, 128.
[19] Maughan B. J., Giles P. A., Rendall S. W., Jones C., Forman W. R. 2012, MNRAS, 421, 1583.
[20] McNamara B. & Nulsen P. 2007, ARA&A, 45, 117.
[21] Morandi A., Ettori S., and Moscardini L. 2007, MNRAS, 379, 518.
[22] Nagai D., Vikhlinin A., and Kravtsov A. V. 2007, ApJ, 655, 98.
[23] Navarro J. F., Frenk C. S., and White S. D. M. 1996, ApJ, 462, 563.
[24] Negri A., Posacki S., Pellegrini S., Ciotti L. 2014, MNRAS, 445, 1351.
[25] Pellegrini S., Ciotti L. and Ostriker J. P. 2012, ApJ, 744, 21.
[26] Pratt G. W., Croston J. H., Arnaud M., Böhringer H. 2009, A&A, 498, 361.
[27] Pulido F. A., McNamara B. R., Edge A. C. et al. 2018, ApJ, 853, 177.
[28] Sarazin C R.. 1997, ASP Conf. Series, 116, 375.
[29] Su Y. & Irwin J. A. 2013, ApJ, 766, 61.
[30] Vikhlinin A., Burenin R. A., Ebeling H. et al. 2009, ApJ, 692, 1033.
[31] Voit G. M. 2005, Rev. Mod. Phys., 77, 207.

Table 1: The list of selected elliptical galaxies

Name	α (J2000)	δ (J2000)	Type	z	D_A Mpc	D_L Mpc	N_H 10^{20} cm^2	T_X keV	L_X 10^{40} erg/s	M_{grav} 10^{12} $M_\odot$
IC1459	4.6590	−64.1096	E3	0.006011	25.503	25.8	1.19	0.70±0.01	2.41±0.06	1.4±0.1
IC4296	313.5384	27.9729	E	0.012465	52.358	53.7	4.11	0.94±0.01	18.11±0.42	5.5±0.8
NGC720	173.0194	−70.3572	E5	0.005821	24.704	25.0	1.55	0.62±0.01	4.11±0.06	0.9±0.1
NGC741	150.9342	−53.6764	E0	0.018549	77.186	80.1	4.47	1.02±0.01	32.75±0.60	4.3±0.2
NGC821	151.5555	−47.5568	E6	0.005787	24.561	24.8	6.34	0.20±0.08	0.10±0.03	0.27±0.2
NGC1404	236.9552	−53.5548	E1	0.006494	27.531	27.9	1.35	0.67±0.04	26.86±10.19	1.4±0.2
NGC1407	209.6362	−50.3838	E0	0.005934	25.179	25.5	5.41	1.02±0.02	5.77±0.13	2.1±0.2
NGC1600	200.4164	−33.2418	E3	0.015614	65.267	67.3	4.71	1.24±0.02	17.14±0.40	7.4±0.8
NGC1700	203.6991	−27.6137	E4	0.012972	54.445	55.9	4.80	0.51±0.02	7.81±0.18	1.3±0.2
NGC2434	281.0002	−21.5444	E0	0.004637	19.716	19.9	12.1	0.59±0.03	0.79±0.04	0.5±0.04
NGC3379	233.4901	57.6328	E1	0.003039	16.112	17.5	2.75	0.24±0.08	0.18±0.02	0.3±0.02
NGC3557	281.5784	21.0890	E3	0.010300	43.410	44.3	7.44	0.43±0.10	4.91±0.67	0.7±0.1
NGC3585	277.2465	31.1753	E6	0.004783	20.332	20.5	5.57	0.32±0.07	0.28±0.03	0.5±0.1
NGC3923	287.2759	32.2224	E4	0.005801	24.620	24.9	6.29	0.58±0.01	5.02±0.06	1.5±0.2
NGC4125	130.1897	51.3391	E6	0.004523	19.234	19.4	1.86	0.49±0.01	1.60±0.03	0.6±0.1
NGC4261	281.8049	67.3726	E2	0.007378	31.236	31.7	1.56	0.80±0.006	6.61±0.08	2.1±0.1
NGC4278	193.7824	82.7727	E1	0.002068	17.11	17.4	1.75	0.33±0.02	0.35±0.01	0.5±0.02
NGC4365	283.8070	69.1819	E3	0.004146	17.642	17.8	1.61	0.44±0.02	0.41±0.02	0.4±0.02
NGC4374	278.2045	74.4784	E1	0.003392	15.527	17.8	2.58	0.81±0.005	5.18±0.05	1.4±0.1
NGC4406	279.0835	74.6369	E3	0.000747	12.578	16.2	2.58	0.88±0.01	10.28±0.24	1.2±0.2
NGC4472	286.9222	70.1961	E2	0.003272	13.125	17.9	1.65	1.06±0.002	18.36±2.08	2.0±0.1
NGC4552	287.9326	74.9668	E0	0.001134	14.512	17.1	2.56	0.64±0.01	2.48±0.04	0.7±0.06
NGC4555	221.8117	86.4343	E	0.022292	92.231	96.4	1.37	1.05±0.02	16.83±0.33	4.1±0.2
NGC4564	289.5604	73.9207	E6	0.003809	15.8	16.3	2.27	0.38±0.15	0.09±0.02	0.5±0.02
NGC4621	294.3646	74.3621	E5	0.001558	13.537	16.3	2.22	0.26±0.07	0.02±0.004	0.3±0.02
NGC4636	297.7485	65.4729	E0	0.003129	14.519	15.2	1.83	0.75±0.003	19.68±1.09	1.0±0.1
NGC4649	295.8736	74.3178	E2	0.003703	14.825	16.9	2.13	0.94±0.003	12.13±1.06	2.0±0.2
NGC4697	301.6329	57.0637	E6	0.00414	17.616	17.8	2.12	0.31±0.01	0.64±0.03	0.3±0.04
NGC4782	304.1379	50.2958	E0	0.015437	64.545	66.6	3.56	1.02±0.01	11.88±0.28	2.4±0.2
NGC4936	306.2037	32.2638	E0	0.010397	43.812	44.7	5.91	0.91±0.04	11.71±0.54	2.3±0.4
NGC5018	309.8982	43.0614	E3	0.009393	39.643	40.4	6.98	0.53±0.07	1.52±0.10	1.3±0.2
NGC5532	357.9614	64.1119	E	0.024704	101.8	106.9	1.86	0.97±0.02	18.02±0.41	5.5±0.3
NGC5813	359.1820	49.8484	E1	0.006525	27.662	28.0	4.23	0.71±0.002	43.88±10.10	0.7±0.1
NGC5846	0.3389	48.9043	E	0.00491	20.867	21.1	4.24	0.79±0.003	15.72±0.11	1.1±0.1
NGC6251	115.7638	31.1958	E	0.024710	101.9	107.0	5.40	0.83±0.03	47.50±1.09	5.2±0.3
NGC6482	48.0905	22.9122	E	0.013129	55.091	56.5	8.04	0.82±0.007	63.39±0.88	1.6±0.2
NGC7176	14.9320	−53.0969	E	0.008376	35.406	36.0	1.61	0.77±0.03	2.51±0.12	2.6±0.3
NGC7196	345.3695	−51.0861	E	0.009750	41.127	41.9	1.84	0.64±0.04	4.81±0.33	2.1±0.4
NGC7618	105.5754	−16.9091	E	0.017309	72.164	74.7	11.9	0.93±0.006	59.50±10.55	3.5±0.2
NGC7626	87.8591	−48.3788	E	0.011358	47.790	48.9	4.94	0.93±0.02	7.19±0.33	2.4±0.3